DOI: 10.1021/ma902770r

Macromolecules
ARTICLE

From Self-Organized Novolac Resins to Ordered Nanoporous Carbons

Di Hu, Zhiguang Xu, Ke Zeng, and Sixun Zheng*

Department of Polymer Science and Engineering and State Key Laboratory of Metal Matrix Composites, Shanghai Jiao Tong University, Shanghai 200240, P. R. China

Received December 16, 2009; Revised Manuscript Received February 9, 2010

ABSTRACT: Polystyrene-*block*-poly(ethylene oxide) (PS-*b*-PEO) diblock copolymer was synthesized and incorporated into novolac resin to obtain the nanostructured phenolic thermosets with hexamethylenetetramine (HMTA) as the curing agent. The morphology of the thermosets were investigated by means of atomic force microscopy (AFM) and small-angle X-ray scattering (SAXS). It was found that long-ranged ordered nanostructures were formed after and before curing reaction. In views of the miscibility of the subchains of the diblock copolymer with the phenol−formaldehyde resins after and before curing reaction, it was judged that the formation of the nanostructures followed the mechanism of self-assembly. In the thermosetting blends, the PEO subchain of the diblock copolymer was miscible with phenolic thermosets after and before cuing reaction. Fourier transform infrared (FTIR) spectroscopy showed that the curing reaction significantly weakened the intermolecular hydrogen-bonding interactions between phenolic matrix and PEO subchains of the diblock copolymer. The nanostructured thermosets were subjected to pyrolysis (and/or carbonization) at elevated temperatures to obtain the nanoporous carbons. The hierarchical nanoporosity of the resulting carbons was confirmed by means of transmission electronic microscopy (TEM), field-emission scanning electronic microscopy (FESEM), and surface-area Brunauer−Emmett−Teller (BET) measurements.

Introduction

The formation of nanophases in multicomponent thermosets can greatly optimize the interactions between modifiers and thermosetting matrix, and thus the properties of materials can be significantly improved.[1] Incorporating amphiphilic block copolymers into thermosets has been proved to be an efficient approach to prepare ordered or disordered nanostructured thermosets.[2,3] Hillmyer et al.[2a,b] first reported the strategy of creating the nanophases in epoxy thermosets via the mechanism of self-assembly. In this protocol, the precursors of thermosets act as the selective solvents of block copolymers, and some self-organized nanophases such as lamellar, bicontinuous, cylindrical, and spherical structures are generated before the curing reaction; these preformed nanophases are fixed via subsequent curing reaction. More recently, it has been demonstrated that ordered and/or disordered nanophases in thermosets can be alternatively formed via the mechanism of reaction-induced microphase separation (RIMS).[3a,b] In this approach, it is not required that the amphiphilic block copolymers are self-organized into the nanophases before curing reaction; i.e., all the subchains of block copolymers may be miscible with precursors of thermosets. Upon curing, a part of subchains of block copolymers are demixed to form the microphases whereas other subchains of the block copolymers remain mixed with the matrix of thermosets. During the past years, there have been a lot of reports on the control of nanostructures in epoxy thermosets.[2,3]

Phenol−formaldehyde (PF) resins are a class of major thermosets, which have widely been employed as molding materials, matrix of composites, adhesive, coatings, and electrical encapsulation materials due to their dimensional stability, high mechanical strength, and chemical resistance.[4a] In addition, PF resins have been used commercially as starting materials to produce glassy carbons with high carbon yields.[4b−i] The widespread application of PF resins motivated the modification of the thermosetting materials via the formation of the nanostructures. Nonetheless, the formation of nanostructures in phenolic thermosets was only occasionally reported vis-à-vis in epoxy thermosets.[5] In terms of the types of PF precursors, the nanostructured phenolic thermosets can be divided into two classes: (i) resols-based and (ii) novolac-based nanocomposites. The resols-based nanocomposites are generally obtained via *in situ* cross-linking of phenol−formaldehyde in the multicomponent mixtures composed of phenol, formaldehyde, water, and amphiphilic block copolymers. Ikkala et al. have ever investigated the formation of nanostructures in the blends of phenol−formaldehyde resols with poly(ethylene oxide)-*block*-poly(propylene oxide)-*block*-poly(ethylene oxide) (PEO-*b*-PPO-*b*-PEO) after removal of water and thermal curing.[5d] Zhao et al. have reported a series of resols-based phenolic thermosets containing amphiphilic block copolymers such as PEO-*b*-PPO-*b*-PEO triblock and polystyrene-*block*-poly(ethylene oxide) (PS-*b*-PEO) diblock copolymers; these phenolic thermosets were further transformed into mesoporous carbons via carbonization reaction at elevated temperatures.[5e,f] It is proposed that in the resols-based phenolic thermosets the formation of nanostructures are significantly affected by several competitive kinetics such as evaporation of solvent (e.g., water), self-assembly of block copolymers, cross-linking, and vitrification of resols. Alternatively, phenolic thermosets can be prepared via the curing of novolac resins. By using novolac precursors, Ikkala and Ruokolaine et al.[5a,b] prepared the nanostructured phenolic thermosets containing the diblock copolymers such as poly(2-vinylpyridine)-*block*-polyisoprene and poly(4-vinylpyridine)-*block*-polystyrene diblock copolymers with hexamethylenetetraamine (HMTA) as the curing agent. It was judged that the formation of the nanostructures in these systems followed the

*To whom correspondence should be addressed: e-mail szheng@sjtu.edu.cn; Tel 86-21-54743278; Fax 86-21-54741297.

 Published on Web 02/24/2010 © 2010 American Chemical Society

self-assembly mechanism. The nanostructured phenolic thermosets containing P4VP-*b*-PS diblock copolymer has been successfully used to access the micro- and mesoporosity in the thermosets by selective removal of PS microdomains via pyrolysis at the maximum temperature of 420 °C.[5b] More recently, Zheng et al.[5c] investigated the morphological evolution in the thermosetting blends of novolac resin with PEO-*b*-PPO-*b*-PEO triblock copolymer, cured with HMTA. It was identified that the formation of nanostructures in the blends of phenolic thermosets containing PEO-*b*-PPO-*b*-PEO followed the mechanism of reaction-induced microphase separation. It was noted that before curing reaction no self-organized nanophases were formed in the blends of novolac resin with PEO-*b*-PPO-*b*-PEO since both PEO and PPO subchains of the triblock copolymer are miscible with novolac resin.

There have been a few reports to deal with the preparation of nanoporous carbons by the use of resols-type phenolic thermosets containing amphiphilic block copolymers[5e,f] while the utilization of novolac-based nanocomposites remains largely unexplored. In this contribution, we reported the formation of nanostructures in phenolic thermosets resulting from the novolac and PS-*b*-PEO diblock copolymer, cured with HMTA. The use of novolac resins instead of resols can allow investigating the morphological evolutions after and before curing reaction and elucidating the formation mechanism of the nanostructures in phenolic thermosets. Thereafter, we explored the preparation of the nanoporous carbons based on the nanostructured thermosets under a long isothermal pyrolysis at the maximum temperature of 800 °C. The morphology and thermal properties of the nanostructured thermosets were investigated by means of atomic force microscopy (AFM) and small-angle X-ray scattering (SAXS). The nanoporosity of the resulting carbons was investigated by means of transmission electronic microscopy (TEM), field emission scanning electronic microscopy (FESEM), and surface-area Brunauer−Emmett−Teller (BET) measurements.

Experimental Section

Materials. Novolac resin was kindly supplied by Rheine Chem Co., Germany, under a trade name of PR95, and it has a quoted molecular weight of M_n = 950. Hexamethylenetetraamine (HMTA) was of analytically pure grade, obtained from Shanghai Reagent Co., China. Styrene (S) is of chemically pure grade and was purchased from Shanghai Reagent Co., China. Prior to use, the inhibitor was removed by washing with aqueous sodium hydroxide (5 wt %) and deionized water for at least three times and dried by anhydrous Na_2SO_4; the monomer was further distilled at reduced pressure. 2-Bromoisobutyryl bromide was purchased from Aldrich Co. and used as received. Copper(I) bromide (CuBr) was purchased from Shanghai Reagent Co., China, and it was purified according to the reported procedure.[6] *N,N,N′,N″,N‴*-Pentamethyldiethylenetriamine (PMDETA) (Aldrich, 99%) was used as received. Poly(ethylene oxide) monomethyl ether (MPEO5000) with a quoted molecular weight of M_n = 5000 was purchased from Fluka Co., Germany, and it was dried by azeotropic distillation with anhydrous toluene prior to use. The model polystyrene with the molecular weight of M_n = 7500 and the polydispersity of M_w/M_n = 1.06 was synthesized in this lab as reported elesewhere.[3b] The solvents such as tetrahydrofuran (THF), dichloromethane, petroleum ether (distillation range: 60−90 °C), and triethylamine (TEA) were of chemical grade, obtained from commercial resources. Prior to use, triethylamine (TEA) was dried over CaH_2 and then was refluxed with *p*-toluenesulfonyl chloride, followed by distillation.

Synthesis of PS-*b*-PEO Diblock Copolymer. 2-Bromoisobutyryl-terminated PEO monomethyl ether (MeO-PEO-Br) was used as a macroinitiator to initiate the polymerization of styrene in the presence of the complex of copper(I) bromide (CuBr) with PMDETA. The PEO macroinitiator was prepared by following the literature method.[7] The PEO monomethyl ether with a quoted molecular weight of M_n = 5000 was used to react with 2-bromoisobutyryl bromide in the presence of triethylamine. To a flask connected with the Schlenk line the MeO-PEO-Br macroinitiator (5.0 g, 1.0 mmol), CuBr (0.1455 g, 1.0 mmol), PMDETA (0.47 g, 3.0 mmol), and styrene (10.0 g, 0.0962 mol) were charged. The reactive mixture was degassed via three pump freeze−thaw cycles and then immersed in a thermostated oil bath at 110 °C. The polymerization was carried out for 24 h, and then the system was cooled to room temperature. Dichloromethane was added to dissolve the product. The reacted mixture was passed over a column of neutral alumina to remove the catalyst; the solution was concentrated and dropped into an excessive amount of petroleum ether to afford the procipitates. The resulting polymer was dried in a vacuum oven at room temperature for 24 h. The polymer (11.034 g) was obtained with the conversion of 60% for styrene monomer. Fourier transform infrared spectroscopy (FTIR) (KBr window): 2928 (C−H, methylene of PEO), 1108 (C−O−C, ether of PEO), 1600, 1580, 1500, and 1450 (C═C of aromatic rings), 2922 (C−H of PS), 3110−3010 (=C−H of aromatic rings). The ^{1}H nuclear magnetic resonance spectroscopy (^{1}H NMR) ($CDCl_3$, ppm): 6.30−7.32 (protons of aromatic rings, 5*H*); 3.61 (−OCH_2CH_2−, 8.4*H*); 1.1−2.1 (protons of methylene and methane of PS subchain, 3*H*). According to the integration intensity of PEO protons to that of PS, the molecular weight of copolymer was calculated to be M_n = 15 600. The curve of gel permeation chromatography (GPC, relative polystyrene standard) displayed an unimodal peak and the molecular weight of M_n = 17 500 and M_w/M_n = 1.1 was determined relative to polystyrene standard.

Preparation of Novolac and PS Binary Blends. The blends of novolac resin and the model PS were prepared by casting from chloroform solution at room temperature. The majority of solvent was evaporated at room temperature for 24 h. To remove the residual solvent, all the blend films obtained were further desiccated *in vacuo* at 30 °C for 48 h.

Preparation of Nanostructured Phenolic Thermosets. The desired amount of PS-*b*-PEO diblock copolymer was added to the preweighted novolac resin; the smallest amount of THF was added with continuous stirring, and then the curing agent HMTA (10 wt % with respect of the quantity of novolac resin) was added to the mixtures with vigorous stirring until homogeneous solutions were obtained. The majority of solvent was evaporated at 60 °C for 12 h, and the residual solvent was eliminated *in vacuo* at 60 °C for 1 h. The curing schedule was set as 100 °C for 2 h plus 150 °C for 2 h and 190 °C for $^1/_2$ h.

Preparation of Nanoporous Carbons. The nanostructured phenolic thermosets containing PS-*b*-PEO diblock copolymer was subjected to pyrolysis in a tube furnace with a multiple-step procedure by following the condition of carbonization reported by Zhao et al.[5f] First, the samples were heated from 150 to 450 °C at the heating rate of 1 °C/min and held at 450 °C for 180 min. The samples were further heated from 450 to 600 °C at the heating rate of 1 °C/min. Thereafter, the temperature was then increased up to 800 °C at the heating rate of 5 °C/min, and the samples were held at 800 °C for 180 min to access a complete carbonization. In all cases, the pyrolysis (and/or carbonization) was carried out in the atmosphere of highly pure nitrogen. The gaseous products during the pyrolysis were purged by the nitrogen at the flow rate of 10 mL s^{-1}.

Measurement and Characterization. *Fourier Transform Infrared Spectroscopy* (*FTIR*). The FTIR measurements were conducted on a Perkin-Elmer Paragon 1000 Fourier transform spectrometer at room temperature (25 °C). The specimens of the films were obtained via casting the chloroform solution of the samples (2 wt %) onto KBr windows. For the samples of thermosets, the powder was mixed with KBr pellets to press into small flakes. All the specimens were

Scheme 1. Synthesis of PS-*b*-PEO Diblock Copolymer

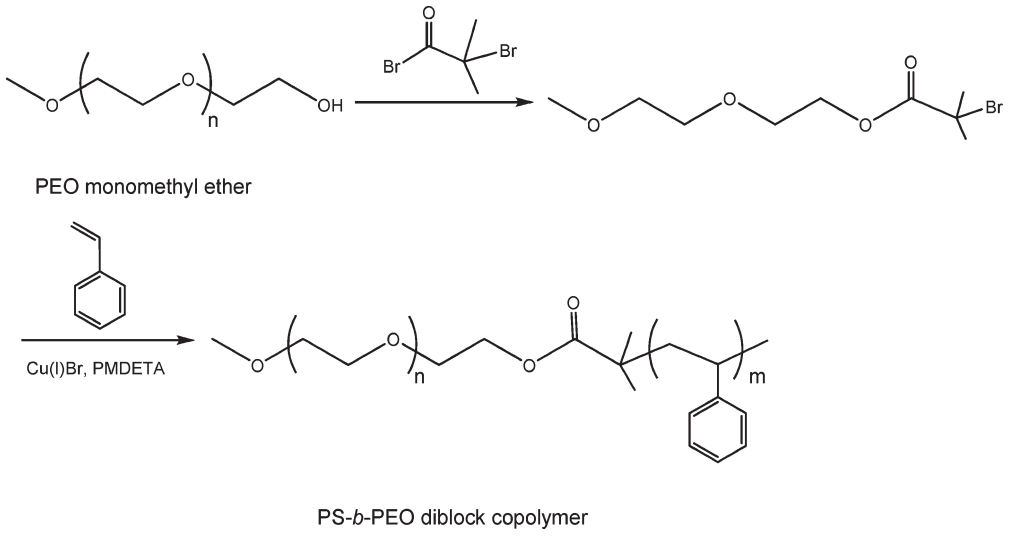

sufficiently thin to be within a range where the Beer–Lambert law is obeyed. In all cases 64 scans at a resolution of 2 cm^{-1} were used to record the spectra.

Nuclear Magnetic Resonance Spectroscopy (*NMR*). The ^1H NMR measurement was carried out on a Varian Mercury Plus 400 MHz NMR spectrometer at 25 °C. The samples were dissolved with deuterated chloroform ($CDCl_3$), and the solutions were measured with tetramethylsilane (TMS) as an internal reference.

Gel Permeation Chromatography (*GPC*). The molecular weights of the polymers were measured on a Perkin-Elmer 200 GPC instrument with a PL mixed-B10m column and a reflective index detector. Polystyrene was used as the standard, and tetrahydrofuran (THF) was used as the eluent at a flow rate of 1 mL/min.

Differential Scanning Calorimetry (*DSC*). The calorimetric measurement was performed on a Perkin-Elmer Pyris 1 differential scanning calorimeter in a dry nitrogen atmosphere. The instrument was calibrated with standard Indium. To remove the thermal history of the samples, a thermal pretreatment was used. All samples (about 10 mg in weight) were heated up to the 100 °C and held at this temperature for 3 min and then quenched to −70 °C. The DSC thermograms were recorded at the heating rate of 20 °C/min. The glass transition temperatures were taken as the midpoint of the capacity transition.

Atomic Force Microscopy (*AFM*). The specimens of thermosets for AFM observation were trimmed using a microtome machine, and the thickness of the specimens is about 70 nm. The morphological observation of the samples was conducted on a Nanoscope IIIa scanning probe microscope (Digital Instruments, Santa Barbara, CA) in tapping mode. A tip fabricated from silicon (125 μm in length with ca. 500 kHz resonant frequency) was used for scan, and the scan rate was 2.0 Hz.

Small-Angle X-ray Scattering (*SAXS*). The SAXS measurements were taken on a Bruker Nanostar system. Two-dimensional diffraction patterns were recorded using an image intensified CCD detector. The experiments were carried out at room temperature (25 °C) using Cu Kα radiation (λ = 1.54 Å, wavelength) operating at 40 kV, 35 mA. The intensity profiles were output as the plot of scattering intensity (I) versus scattering vector, $q = (4/\lambda)\sin(\theta/2)$ (θ = scattering angle).

Transmission Electronic Microscopy (*TEM*). The carbons were imbedded in epoxy thermosets (i.e., the formulation of diglycidyl ether of bisphenol A with tetraethylenepentamine cured at 100 °C for 2 h). The epoxy thermosets were trimmed using a microtome machine; the thickness of the specimens is about 70 nm. Then the ultrathin sections were placed on 200 mesh copper grids for observation. Transmission electron microscopy analyses were performed on a JEOL JEM-2010 high-resolution transmission electron microscopy at an acceleration voltage of 120 kV.

Scanning Electron Microscopy (*SEM*). In order to observe the morphology, the carbons were fractured and the surfaces of the fractured ends were coated with thin layers of gold of about 70 Å. The morphological structures were observed with a JEOL JSM 7401F field emission scanning electron microscope (FESEM) at an activation voltage of 5 kV.

Specific Surface Area Analyses. Surface areas and pore size distributions were determined by nitrogen sorption at 77 K using the volumetric technique on a Micromeritics ASAP 2010 instrument (Norcross, GA). Specific surface areas were calculated using the multipoint Brunauer–Emmett–Teller (BET) method using DeltaGraph graphics software. Pore size distributions were determined by density functional theory (DFT) using nitrogen on carbon at 77 K with the slitlike pore model.

Results and Discussion

Synthesis of PS-*b*-PEO Diblock Copolymer. The synthetic route of PS-*b*-PEO diblock copolymer is shown in Scheme 1. First, the poly(ethylene oxide) monomethyl ether (MeO–PEO–OH) (M_n = 5000) was reacted with 2-bromoisobutyryl bromide to obtain 2-bromoisobutyryl-terminated PEO monomethyl ether [MeO–PEO–OOCCBr$(CH_3)_2$], which was used as the macroinitiaor to perform the atom transfer radical polymerization (ATRP) of styrene in the presence of the complex of Cu(I)Br and *N*,*N*,*N*′,*N*″,*N*‴-pentamethyldiethylenetriamine (PMDETA). The conversion of styrene was controlled within 60% to obtain the copolymer with the desired molecular weight. The product was subjected to ^1H nuclear magnetic resonance spectroscopy (NMR), and the ^1H NMR spectrum is shown in Figure 1. The resonance of aromatic protons in the PS subchain of the diblock copolymer appeared in the range of 6.30–7.32 ppm, and the resonance at 1.40 and 1.85 ppm was assignable to the protons of methylene and methane groups of PS block. The intense resonance of ethylene protons for PEO subchain appeared at 3.65 ppm. According to the ratio of integration intensity of ethylene protons for PEO block to that of ethylene (or aromatic ring) protons of PS block, the length of PS block was estimated to be M_n = 10 600 with the PEO block length of M_n = 5000. The diblock copolymer was subjected to gel permeation

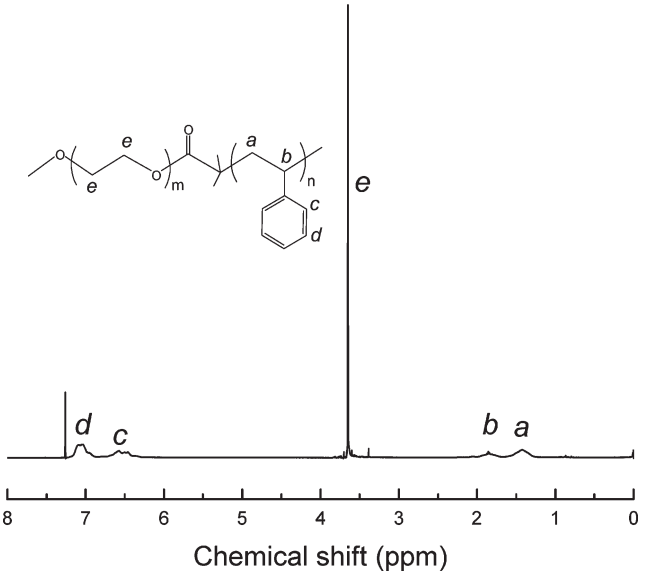

Figure 1. ^{1}H NMR spectrum of PEO-*b*-PS diblock copolymer.

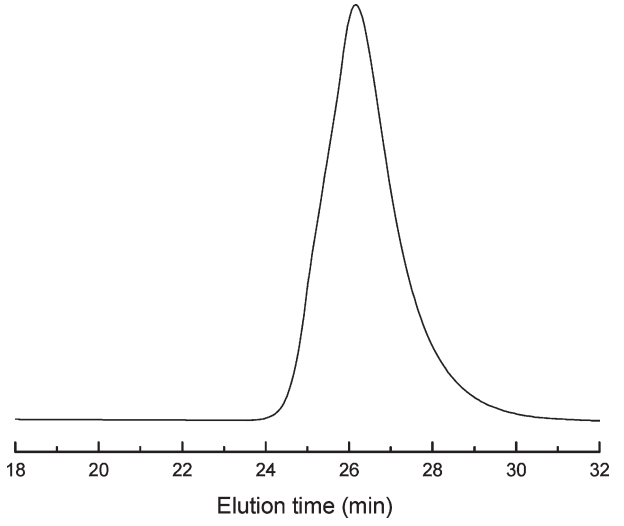

Figure 2. GPC curve of PEO-*b*-PS diblock copolymer.

chromatography (GPC), and the GPC curve is shown in Figure 2. It is seen that the block copolymer displayed a unimodal peak, indicating that no homopolymer was produced with the polymerization of styrene. The GPC measurment gave the molecular weight of diblock copolymer to be M_n = 17 500 with M_w/M_n = 1.10. The ^{1}H NMR and GPC indicate that the PS-*b*-PEO diblock copolymer was successfully synthesized.

Nanostructures in Phenolic Thermosets. There have been a few reports on the formation of nanostructures in HMTA-cured phenolic thermosets containing block copolymers such as poly(2-vinylpyridine)-*block*-polyisoprene (P2VP-*b*-PI) diblock,[5a] poly(4-vinylpyridine)-*block*-polystyrene (P4VP-*b*-PS) diblock,[5b] and poly(ethylene oxide)-*block*-poly(propylene oxide)-*block*-poly(ethylene oxide) (PEO-*b*-PPO-*b*-PEO) triblock copolymers.[5c] It has been noted that chemical composition and molecular weight of block copolymers have a profound effect on phase behavior of the thermosetting blends. In the present case, the PS-*b*-PEO diblock copolymer was utilized to control the formation of the nanostructures in its blends with phenolic thermosets.

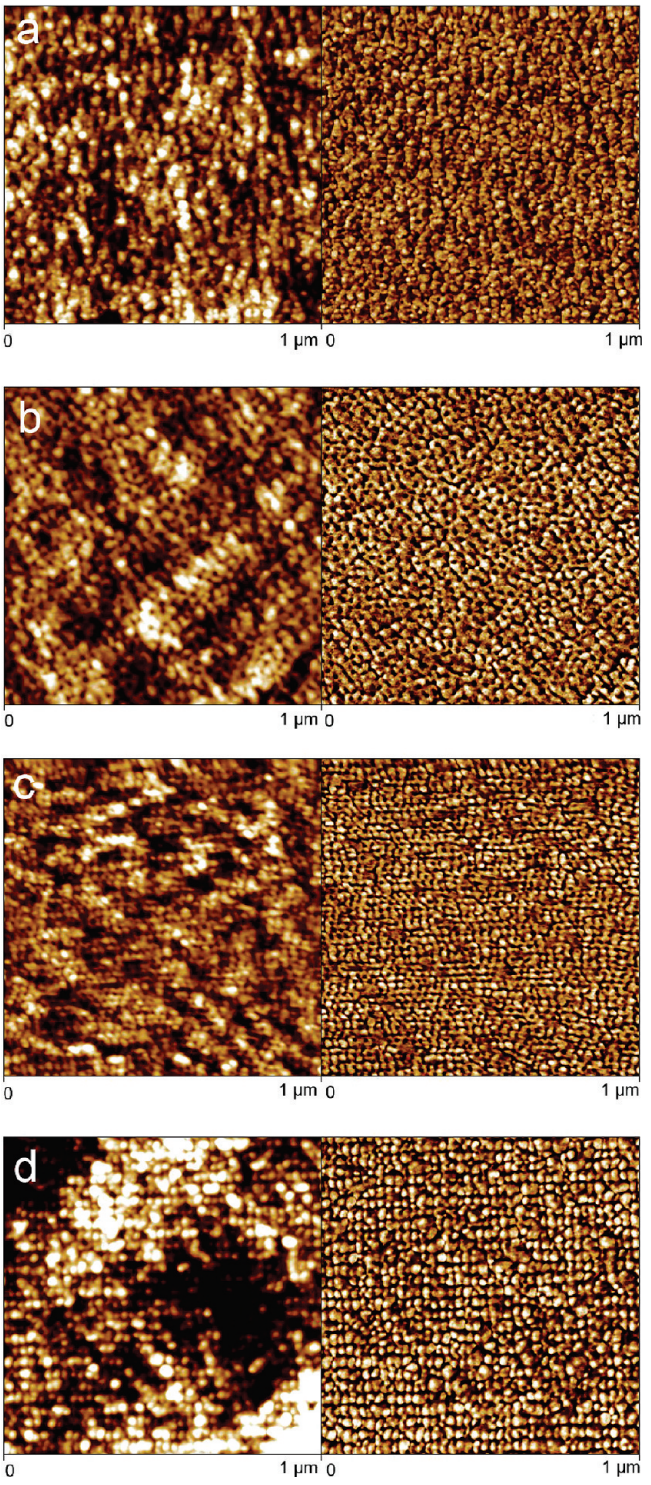

Figure 3. AFM images of nanostructured phenolic thermosets containing: (a) 10, (b) 20, (c) 30, and (d) 40 wt % of PEO-*b*-PS diblock copolymer. Left: topography; right: phase contrast images.

Before curing, all the ternary mixtures composed of novolac, HMTA, and PS-*b*-PEO diblock copolymer were homogeneous and transparent. After cured at the elevated temperatures, the thermosetting blends still remained homogeneous and transparent. The clarity suggests that no macroscopic phase separation occurred at the scale exceeding the wavelength of visible light after and before curing reaction. The thermosetting phenolic blends were obtained with the content of PS-*b*-PEO diblock copolymer up to 40 wt %. The

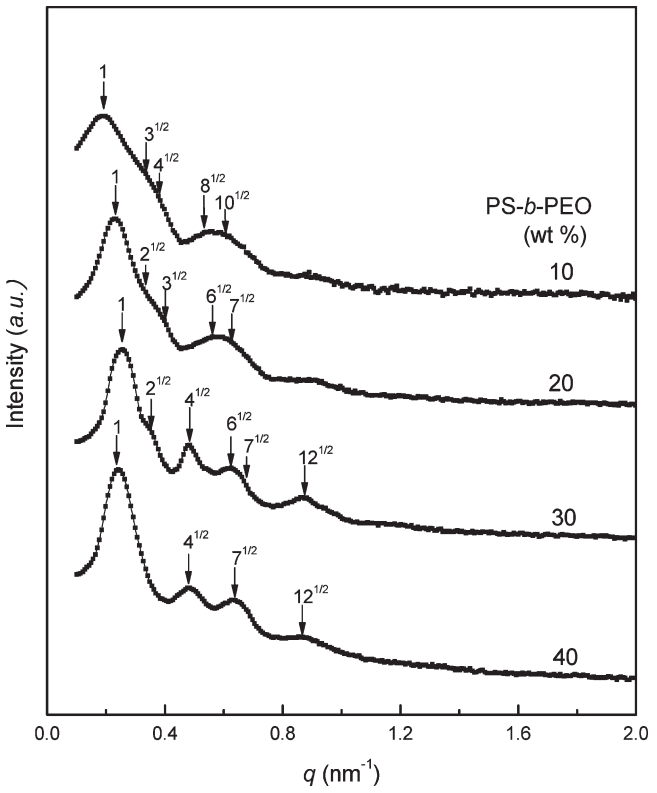

Figure 4. SAXS profiles of the nanostructured phenolic thermosets containing PEO-*b*-PS diblock copolymer. Each profile has been shifted vertically for clarity.

phenolic thermosets containing PS-*b*-PEO diblock copolymer were trimmed using an ultrathin microtome machine, and the sections were subjected to the morphological observations by means of atomic force microscopy (AFM). Shown in Figure 3 are the AFM micrographs of the thermosets containing 10, 20, 30, and 40 wt % PS-*b*-PEO diblock copolymer. The left and right images are the topography and phase contrast images, respectively. The topography images showed that the surfaces of the as-prepared specimens are free of visible defects, and thus the effect of roughness resulting from the specimen preparation on morphology can be negligible. It is noted that all the thermosetting blends possess nanostructured morphologies. In terms of the volume fraction of PS and the difference in viscoelastic properties between phenolic matrix and PS phases, the light continuous regions are assignable to the cross-linked phenolic matrix, which was miscible with the PEO subchains of the block copolymer while the dark regions are attributed to PS domains. The separate PS particles were imbedded in the continuous phenolic matrix at the average size of ca. 20−30 nm in diameter, and the size of PS nanophases almost remained invariant with increasing the content of PS-*b*-PEO. The interdomain distance decreased with increasing the content of PS-*b*-PEO diblock copolymer (see Figure 3a−d). It is of interest to note that in all cases the PS nanophases were arranged into ordered structures. The order of the nanostructures increased with increasing the concentration of PS-*b*-PEO diblock copolymer. The ordered nanostructures were further investigated by means of small-angle X-ray scattering (SAXS).

Shown in Figure 4 are the SAXS profiles of the phenolic thermosets containing 10, 20, 30, and 40 wt % PS-*b*-PEO diblock copolymer. It is seen that the well-defined multiple scattering peaks were observed in all the cases, indicating that the thermosets are microphase-separated and the microphase-separated nanostructures were to some extent long-ranged ordered. According to the position of each first-order scattering peak, the Bragg's spacing d_m values were obtained to be 33.2, 27.8, 25.1, and 26.1 nm for the thermosets containing 10, 20, 30, and 40 wt % of PS-*b*-PEO diblock copolymer, respectively. It is noted that the positions of the first-order scattering peaks slightly shifted to the higher q values with increasing the content of PS-*b*-PEO diblock copolymer, suggesting that the average distance between neighboring domains decreased with increasing the content of the diblock copolymer. The slight shifts of the scattering maxima could be associated with local rearrangement, leading to an enhancement of the long-range order. This result is in a good agreement with those obtained by means of AFM. For the thermoset containing 10 wt % PS-*b*-PEO diblock copolymer, the scattering peaks at the q values of 1, $3^{0.5}$, $4^{0.5}$, $8^{0.5}$, and $10^{0.5}$ relative to the first-order scattering peak positions (q_m) are discernible, implying that the spherical nanodomains could be arranged into body-centered cubic (bcc) lattice. The similar morphology was also detected for the thermoset containing 20 wt % PS-*b*-PEO diblock copolymer, as indicated by the presence of the scattering peaks at the q values of $2^{0.5}$, $3^{0.5}$, $6^{0.6}$, and $7^{0.5}$ relative to the first-order scattering peak position. While the content of PS-*b*-PEO diblock copolymer is 30 wt %, the hexagonal cylindrical lattice appeared as evidenced by the scattering peaks at the q values of $4^{0.4}$, $7^{0.4}$, and $12^{0.5}$ relative to the first-order scattering peak position. In the mean time, the scattering peaks characteristic of bcc lattice are still discerned at the q values of $2^{0.5}$ and $6^{0.5}$ relative to the first-order scattering peak position. Therefore, the thermoset containing 30 wt % PS-*b*-PEO diblock copolymer could display the morphology which combined hexagonal cylindrical and bcc lattices. While the content of PS-*b*-PEO diblock copolymer was increased up to 40 wt %, the PS nanodomains were almost arranged into the hexagonal cylindrical lattices, as evidenced by the appearance of the scattering peaks at the q values of $4^{0.5}$, $7^{0.5}$, and $12^{0.5}$ relative to the first-order scattering peak position.

Formation Mechanism of Nanostructures. Depending on the miscibility and phase behavior of the subchains of block copolymers with thermosets after and before curing reaction, the formation of nanostructures in thermosets containing amphiphilic block copolymers could follow either self-assembly or reaction-induced microphase separation mechanism.[2a,2b,3a,3b] For the approach of self-assembly, the precursors of thermosets act as selective solvents of block copolymers and self-organized nanostructures (i.e., micelle) are formed prior to curing, and these nanostructures are further locked in with subsequent curing reaction. For reaction-induced microphase separation approach, it is not required that the amphiphilic block copolymers are self-organized into the nanophases before curing reaction; i.e., all the subchains of block copolymers may be miscible with precursors of thermosets. Upon curing, a part of subchains of block copolymers are demixed to form the microphases whereas other subchains of the block copolymer remain mixed with the matrix of thermosets.

In the present case, it is important to know the miscibility and phase behavior of the blends of the subchains of diblock copolymers with phenolic resin after and before curing reaction for the judgment of the formation mechanism of the nanostructures. The miscibility of novolac resin and PEO blends cured with HMTA has been previously reported by Zhong et al.,[8] and it has been demonstrated that the thermosetting blends of novolac and PEO are miscible after and

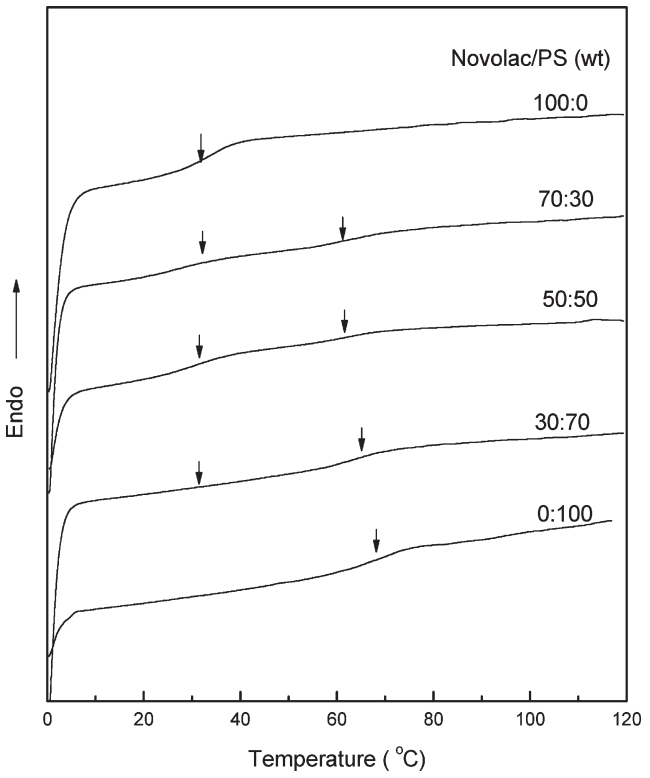

Figure 5. DSC curves of novolac, PS, and their blends.

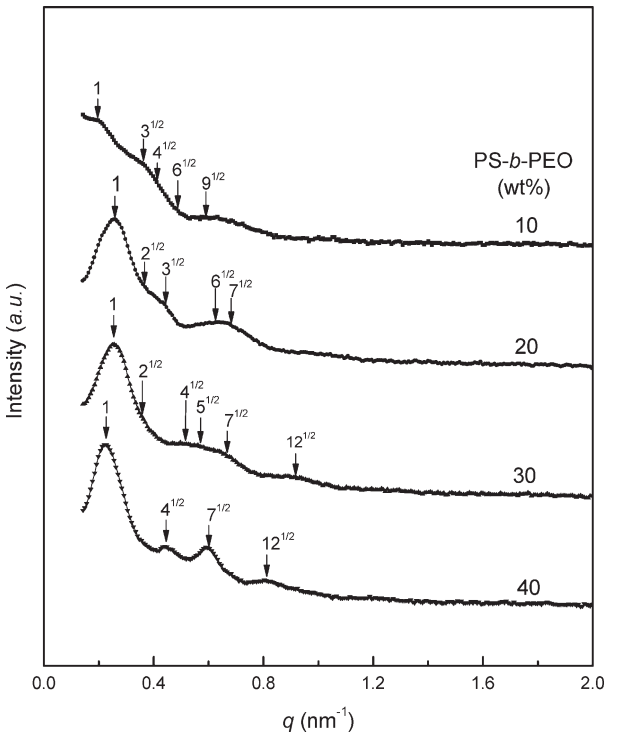

Figure 6. SAXS profiles of the binary blends of phenolic and PEO-*b*-PS diblock copolymer before curing. Each profile has been shifted vertically for clarity.

before curing. In this work, the miscibility of novolac blends with PS before curing was readily investigated by means of differential scanning calorimetry (DSC). The model PS having the identical molecular weight with the length of PS in the PS-*b*-PEO diblock copolymer was used to prepare its blends with novolac resin, and the DSC curves of novolac resin blends with the model PS are shown in Figure 5. The novolac precursor displayed the glass transition at 30 °C whereas the model PS at 70 °C. It should be pointed out that the T_g (~70 °C) of the model PS is lower than that of normal PS (~100 °C), owing to its lower molecular weight (M_n = 7500). It is seen that the range of composition investigated each blend displayed two separate glass transition temperatures (T_g's), assignable to novolac- and PS-rich phase, respectively. It is noted that the T_g's of novolac-rich phase remain almost invariant whereas those of PS-rich phase slightly lower than that of the model PS and decreased with increasing the content of the model PS. This observation indicates that in a small amount of novolac resin could be mixed with the model PS in the PS-rich phase. The appearance of two separate T_g's indicates that PS is immiscible with novolac resin before curing reaction.

The immiscibility of PS with novolac resin suggests that the self-organized nanostructures could be formed in the blends of novolac resin with PS-*b*-PEO diblock copolymer before curing reaction. The self-assembly behavior of PS-*b*-PEO diblock copolymer in novolac blends were readily investigated by means of small-angle X-ray scattering (SAXS). The SAXS profiles of the blends of novolac resin with PS-*b*-PEO diblock copolymer are presented in Figure 6. The well-defined scattering peaks were exhibited in all the cases, indicating that the blends are microphase-separated. It is noted that in all the cases the blends containing PS-*b*-PEO diblock copolymer also displayed the multiple scattering maxima as denoted with the arrows, indicating that the phenolic thermosets possess long-range ordered nanostructures. Compared to the SAXS profiles of the phenolic thermosets, it is found that before curing reaction the PS nanodomains in the blends were arranged into the lattices similar to those in the thermosetting blends containing PS-*b*-PEO diblock copolymer; i.e., the curing reaction did not significantly change the self-organized structures. Nonetheless, it is noted the degree of ordering of the nanostructures prior to curing reaction is much lower than that in the phenolic thermosets containing PS-*b*-PEO diblock copolymer. It is proposed that the curing reaction is favorable to promote the ordered arrangement of the PS nanophases in the phenolic matrix. According to the positions of the first-order scattering peaks, the Bragg's spacing d_m can be obtained to be 30.3, 24.9, 24.7, and 28.0 nm for the blends containing 10, 20, 30, and 40 wt % PS-*b*-PEO diblock copolymer, respectively. It is noted that with the inclusion of the curing agent (viz. HMTA) and curing at elevated temperature the Bragg's spacing d_m increased. The increased Bragg's spacing could be ascribed to the increased volume fraction of phenolic thermosets resulting from the inclusion of 10% HMTA. In addition, the demixing of novolac from the PS-rich nanodomains induced by the curing reaction would give rise to the decrease in the size of PS domains, which also contributed to the increased principal domain spacing.

Effect of Curing on Hydrogen-Bonding Interactions. It is the miscibility of PEO subchain of the diblock copolymer with novolac resin after and before curing reaction that suppress the macroscopic phase separation of the block copolymer from the thermosetting blends with the occurrence of curing reaction. The miscibility is responsible for the formation of the intermolecular hydrogen-bonding interactions between novolac resin and PEO. Nonetheless, the intermolecular hydrogen-bonding interactions could be significantly affected by the curing reaction owing to the formation of three-dimensional cross-linked networks. The hydrogen-bonding interactions were readily investigated by

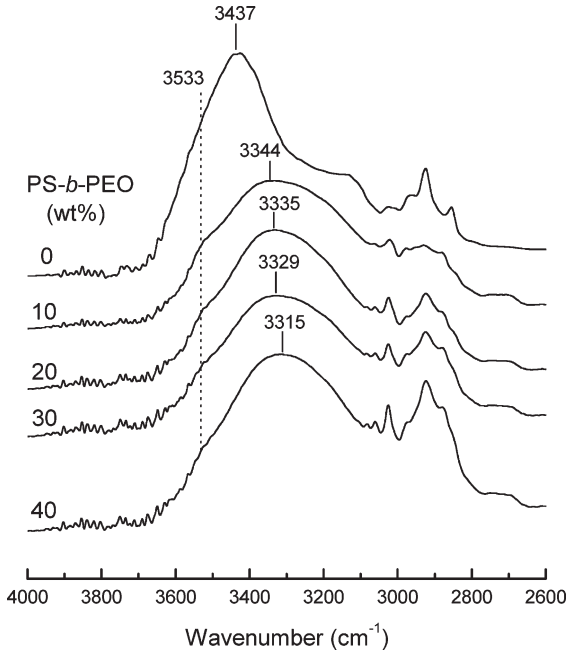

Figure 7. FTIR spectra of the blends of novolac resin with PS-*b*-PEO diblock copolymer.

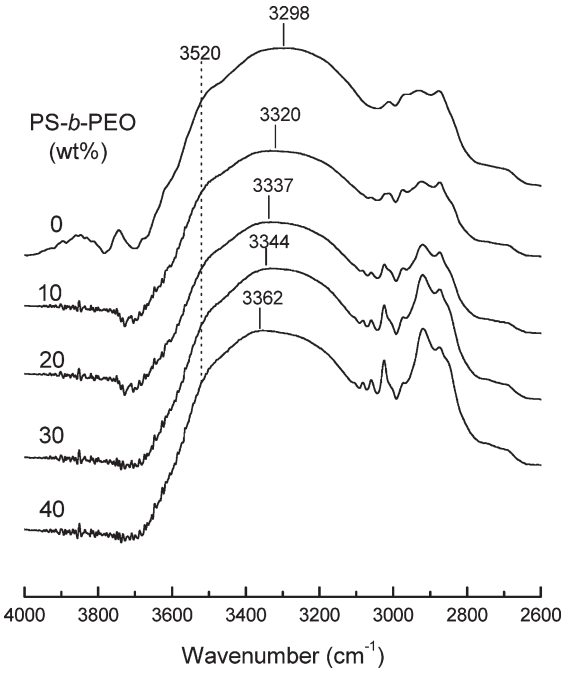

Figure 8. FTIR spectra of the nanostructured phenolic thermosets containing PS-*b*-PEO diblock copolymer.

means of Fourier transform infrared spectroscopy (FTIR). Shown in Figure 7 are the FTIR spectra of the blends of novolac resin with PS-*b*-PEO diblock copolymer before the curing reaction. The pure novolac was characteristic of the stretching vibration of phenolic hydroxyl groups at 3437 cm^{-1}; this band was attributed to self-associated hydroxyls, and the width of the band reflects the broad distribution of hydrogen-bonded hydroxyl stretching frequencies. The stretching vibration of free phenolic hydroxyl groups occurred at 3533 cm^{-1}; it is seen that the band became increasingly pronounced upon adding the diblock copolymer to the system. The frequency difference ($\Delta\nu$) between free and H-bonded hydroxyl bands can be taken as a measure of the average strength of the intermolecular interactions.[9] For the pure novolac resin, the $\Delta\nu$ value is 96 cm^{-1}. After the diblock copolymer was added to the system, the value was increased up to $\Delta\nu$ = 218 cm^{-1} for the blend containing 40% PS-*b*-PEO diblock copolymer. The increased $\Delta\nu$ values suggests that the strength of intermolecular hydrogen-bonding interactions in the blends of novolac resin with PS-*b*-PEO (i.e., PEO subchains) is much stronger than the self-association of phenolic hydroxyl groups in the pure novolac resin.

With adding HMTA and curing at elevated temperatures, the blends underwent a series of structural changes involving chain extension, branching and cross-linking in succession, and the nanostructured thermosets were obtained. Shown in Figure 8 are the FTIR spectra of the nanostructured phenolic thermosets containing PS-*b*-PEO diblock copolymer in the region of 2600−4000 cm^{-1}. With the occurrence of curing reaction, the hydrogen-bonded hydroxyl bands are observed to shift to higher frequencies with increasing the content of PS-*b*-PEO diblock copolymer. It is noted that the formation of the cross-linked networks significantly affected the intermolecular hydrogen-bonding interactions. For the control phenolic thermoset, the $\Delta\nu$ value was 222 cm^{-1}. It is of interest to note that the $\Delta\nu$ value of the pure phenolic thermoset was significantly higher than that of uncured novolac resin (viz. 96 cm^{-1}), implying that the self-association of phenolic hydroxyl groups in the pure phenolic thermoset are much stronger than that in the novolac resin. It is plausible to propose that the formation of the tightly cross-linked networks facilitate the self-association of phenolic hydroxyl groups. Nonetheless, it is worth noticing that for the nanostructured phenolic thermosets containing PS-*b*-PEO diblock copolymer the $\Delta\nu$ value was diminished to 158 cm^{-1} when the content of PS-*b*-PEO diblock copolymer is 40 wt % with the occurrence of the curing reaction. The decreased $\Delta\nu$ values suggest that the intermolecular hydrogen-bonding interactions between the phenolic thermosets and PEO subchains were significantly weakened, owing to the occurrence of the curing reaction. In the thermosetting polymer blends, it is proposed that the formation of the three-dimensional cross-linking network could reduce the intermolecular hydrogen-bonding interactions among hydroxyl groups of phenolic thermosets versus ether oxygen atoms of PEO.[10] FTIR spectroscopy indeed shows that there were still the intermolecular hydrogen-bonding interactions between phenolic hydroxyl groups and ether oxygen atoms of PEO subchains after curing reaction although the strength of the intercomponent hydrogen-bonding interactions were significantly reduced. It is the intercomponent hydrogen-bonding interactions that suppressed the occurrence of macroscopic phase separation.

Formation of Nanoporosity in Carbons. Nanoporous carbons are of great interest for a variety of applications including gas separation, water purification, catalyst supports and electrodes for batteries and fuel cells[11]. In this work, the nanoporosity can be generated by a two-step procedure of pyrolysis (and/or carbonization). In the first step, the nanostructured thermosets was pyrolyzed at lower temperatures (viz. 450 °C) for 180 min selectively to remove the PS nanodomains in the microphase-separated thermosets to form the nanoporous backbones of the thermosets.[5b] After that, the samples were further heated up to higher temperatures (viz. 800 °C) for 180 °C to obtain the carbonized products.[4i] With the process of pyrolysis and carbonization, the PS nanodomains dispersed in the phenolic matrices were removed, and the matrices composed of PEO block and phenolic thermosets were decomposed to

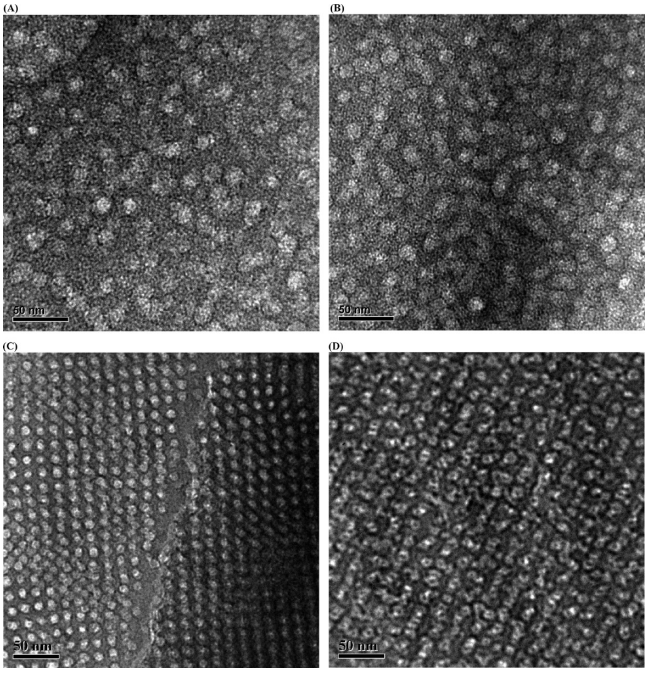

Figure 9. TEM micrographs of the nanoporous carbon prepared from the nanostructured phenolic thermosets containing (A) 10, (B) 20, (C) 30, and (4) 40 wt % PS-*b*-PEO diblock copolymer.

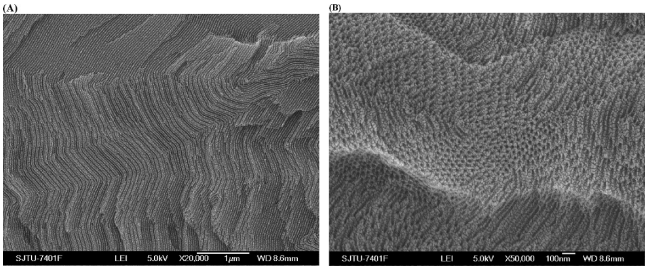

Figure 10. FESEM micrographs of the nanoporous carbon prepared from the nanostructured phenolic thermoset containing 40 wt % PS-*b*-PEO diblock copolymer: (A) overall view; (B) morphology of intersection.

some extent. The removal of PS nanophases contributed to the formation of the nanopores (or mesopores) with the size of 2−50 nm in diameter, whereas the decomposition of PEO together with the release of gaseous matter from phenolic matrices could result in the microporosity with the size lower than 2 nm. It should be pointed out that the partial collapse of the pores occurred with the process of pyrolysis and carbonization.

The formation of nanoporosity was investigated by means of transmission electron microscopy (TEM). Shown in Figure 9 are the TEM micrographs of the as-prepared carbon materials. It is seen that all the carbons displayed the nanoporous structures. For the carbon from the nanostructured thermoset containing 10 wt % PS-*b*-PEO diblock copolymer, the spherical pores were dispersed in the continuous carbon matrix at the size of 10−20 nm (Figure 9A). The quantity of pores increased with increasing the content of PS-*b*-PEO diblock copolymer (Figure 9B). It is seen that the ordered nanoporous structures were displayed when the content of PS-*b*-PEO diblock copolymer is 20 wt % or higher (see Figure 9B−D). For the carbon from the thermoset containing 30 wt % PS-*b*-PEO diblock copolymer, the spherical nanopores were arranged into cubic lattice whereas

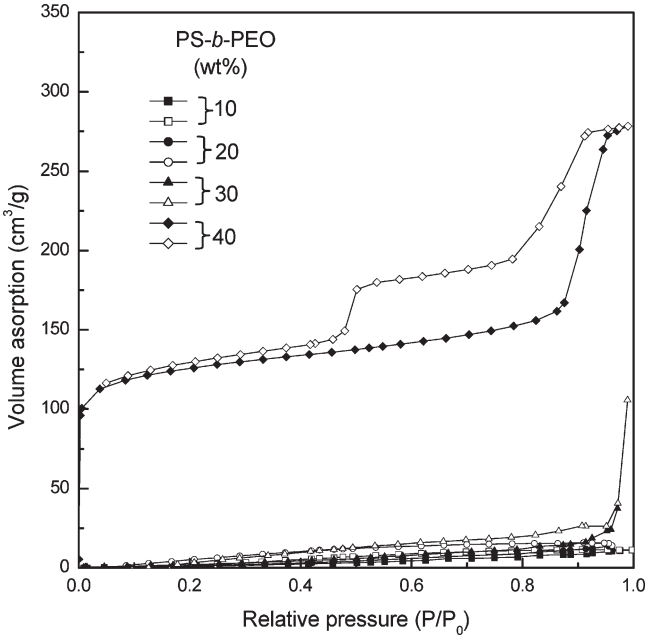

Figure 11. Nitrogen sorption isotherms of the nanoporous carbons: solid symbols, adsorption; open symbols, desorption.

a hexagonal cylindrical lattice was discernible for the carbon materials from the thermosets containing 40 wt % PS-*b*-PEO diblock copolymer. The large-scale ordered nanoporosity in the carbon materials was further confirmed by field emission scanning electron microscopy (FESEM). Shown in Figure 10 are the FESEM micrographs of the carbon from the nanostructured thermoset containing 40 wt % PS-*b*-PEO diblock copolymer. It is seen that the carbon possessed the large-scale cylindrical porous (or hierarchical) structure (Figure 10A). In some regions, the orientation direction of the cylinder axes is approximately parallel to the surface of fractured ends (Figure 10B). The results of TEM and SEM indicate that the nanoporosity in the carbon materials was survived during the carbonization at the elevated temperature as high as 800 °C for 3 h. Nonetheless, it is noted that there was the volume shrinkage of the nanodomains by comparing the morphology of the thermosets with that of the carbons with the process of pyrolysis and carbonization (see Figures 3 and 9). It is plausible to propose that the volume shrinkage of the nanodomains is attributed to the partial collapse of the micropores with the process of pyrolysis and carbonization.

The porosity of the carbon materials was measured by the experiments of nitrogen sorption. Shown in Figure 11 are the nitrogen sorption isotherms of the nanoporous carbon materials. These materials exhibited IV sorption isotherms with a H_2-type hysteresis loop, suggesting that the materials possessed some caged pores with small windows. For the carbon from the nanostructured thermoset containing 40 wt % PS-*b*-PEO diblock copolymer two steps were observed in the desorption branches at the values of relative pressure (P/P_0) of 0.5 and 0.8, which are characteristic of a broad capillary condensation of nitrogen in the sample. From the adsorption branches of the nitrogen sorption isotherms, the Brunauer−Emmett−Teller (BET) surface areas are calculated to be 12.8, 15.1, 29.3, and 168.3 m^2/g for the carbons from the thermosets containing 10, 20, 30, and 40 wt % PS-*b*-PEO diblock copolymer, respectively, as shown in Figure 12. The BET surface areas increased with increasing the content of PS-*b*-PEO diblock copolymer. It is worth noticing that while

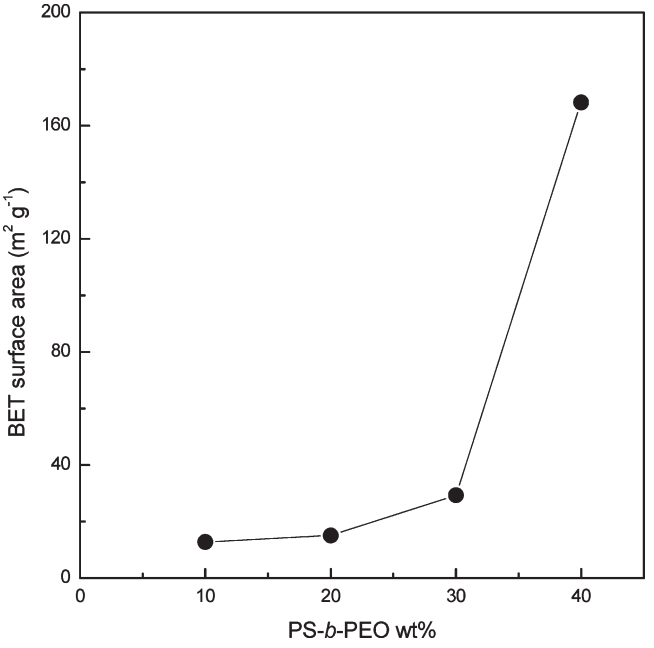

Figure 12. Plot of BET surface areas of the nanoporous carbons as a function of the content of PS-*b*-PEO diblock copolymer in the nanostructured thermosets.

the content of PS-*b*-PEO diblock copolymer is lower than 30 wt %, the BET surface areas were lower than 30 m^2/g. However, an abrupt increase in BET surface area was found for the nanoporous carbon from the nanostructured thermoset containing 40 wt % PS-*b*-PEO diblock copolymer, and the BET surface area was as high as 168 m^2/g. This observation could be associated with the formation of the interconnected nanosized tunnels in the carbon; i.e., the hierarchical nanoporosity was obtained (see Figure 10).

Conclusions

Polystyrene-*block*-poly(ethylene oxide) (PS-*b*-PEO) diblock copolymer was synthesized and incorporated into novolac resin to obtain the nanostructured phenolic thermosets. The nanostructures of the thermosets were investigated by means of atomic force microscopy (AFM) and small-angle X-ray scattering (SAXS). It was found that long-ranged ordered nanostructures were formed after and before curing reaction. In views of the miscibility of the subchains of the diblock copolymer with the phenol−formaldehyde resins, it was judged that the formation of nanostructures in the thermosets followed the mechanism of self-assembly. In the thermosetting blends, the PEO subchain of the diblock copolymer was miscible with phenolic thermosets after and before cuing reaction. However, Fourier transform infrared (FTIR) spectroscopy showed that the curing reaction significantly weakened the intermolecular hydrogen-bonding interactions between phenolic matrix and PEO subchains of the diblock copolymer. The nanostructured thermosets were subjected to pyrolysis (viz. carbonization) at elevated temperatures to obtain the nanoporous carbons. The hierarchical nanoporosity of the resulting carbons was confirmed by means of transmission electron microscopy (TEM), field-emission scanning electronic microscopy (FESEM), and surface-area Brunauer−Emmett−Teller (BET) measurements.

Acknowledgment. Financial support from Natural Science Foundation of China (No. 20474038 and 50873059) and National Basic Research Program of China (No. 2009CB930400) is gratefully acknowledged. The authors also thank the Shanghai Synchrotron Radiation Facility under the project of 08sr0157 and Shanghai Leading Academic Discipline Project (Project No. B202) for partial support.

References and Notes

(1) (a) de Gennes, P.-G. *Scale Concepts in Polymer Physics*; Cornell University Press: Ithaca, NY, 1979. (b) de Gennes, P.-G. *Phys. Lett.* **1969**, *28A*, 725. (c) Ruiz-Pérez, L.; Royston, G. J.; Fairclough, J. A.; Ryan, A. J. *Polymer* **2008**, *49*, 4475. (d) Pascault, J. P.; Williams, R. J. J. In *Polymer Blends*; Paul, D. R., Bucknall, C. B., Eds.; Wiley: New York, 2000; Vol. *1*, pp 379−415. (e) Zheng, S. In *Epoxy Polymers: New Materials and Innovations*; Pascault, J. P., Williams, R. J. J., Eds.; Wiley-VCH: Weinheim, 2010; pp 79−108.

(2) (a) Hillmyer, M. A.; Lipic, P. M.; Hajduk, D. A.; Almdal, K.; Bates, F. S. *J. Am. Chem. Soc.* **1997**, *119*, 2749. (b) Lipic, P. M.; Bates, F. S.; Hillmyer, M. A. *J. Am. Chem. Soc.* **1998**, *120*, 8963. (c) Mijovic, J.; Shen, M.; Sy, J. W.; Mondragon, I. *Macromolecules* **2000**, *33*, 5235. (d) Grubbs, R B.; Dean, J. M.; Broz, M. E.; Bates, F. S. *Macromolecules* **2000**, *33*, 9522. (e) Dean, J. M.; Lipic, P. M.; Grubbs, R. B.; Cook, R. F.; Bates, F. F. *J. Polym. Sci., Part B: Polym. Phys.* **2001**, *39*, 2996. (f) Guo, Q.; Thomann, R.; Gronski, W. *Macromolecules* **2002**, *35*, 3133. (g) Ritzenthaler, S.; Court, F.; Girard-Reydet, E.; Leibler, L.; Pascault, J. P. *Macromolecules* **2002**, *35*, 6245. (h) Ritzenthaler, S.; Court, F.; Girard-Reydet, E.; Leibler, L.; Pascault, J. P. *Macromolecules* **2003**, *36*, 118. (i) Rebizant, V.; Abetz, V.; Tournihac, T.; Court, F.; Leibler, L. *Macromolecules* **2003**, *36*, 9889. (j) Dean, J. M.; Verghese, N. E.; Pham, H. Q.; Bates, F. S. *Macromolecules* **2003**, *36*, 9267. (k) Rebizant, V.; Venet, A. S.; Tournillhac, F.; Girard-Reydet, E.; Navarro, C.; Pascault, J. P.; Leibler, L. *Macromolecules* **2004**, *37*, 8017. (l) Dean, J. M.; Grubbs, R. B.; Saad, W.; Cook, R. F.; Bates, F. S. *J. Polym. Sci., Part B: Polym. Phys.* **2003**, *41*, 2444. (m) Wu, J.; Thio, Y. S.; Bates, F. S. *J. Polym. Sci., Part B: Polym. Phys.* **2005**, *43*, 1950. (n) Zucchi, I. A.; Galante, M. J.; Williams, R. J. J. *Polymer* **2005**, *46*, 2603. (o) Thio, Y. S.; Wu, J.; Bates, F. S. *Macromolecules* **2006**, *39*, 7187. (p) Serrano, E.; Tercjak, A.; Kortaberria, G.; Pomposo, J. A.; Mecerreyes, D.; Zafeiropoulos, N. E.; Stamm, M.; Mondragon, I. *Macromolecules* **2006**, *39*, 2254. (q) Ocando, C.; Serrano, E.; Tercjak, A.; Peña, C.; Kortaberría, G.; Calberg, C.; Grignard, B.; Jerome, R.; Carrasco, P. M.; Mecerreyes, D.; Mondragon, I. *Macromolecules* **2007**, *40*, 4086. (r) Maiez-Tribut, S.; Pascault, J. P.; Soulé, E. R.; Borrajo, J.; Williams, R. J. J. *Macromolecules* **2007**, *40*, 1268. (s) Gong, W.; Zeng, K.; Wang, L.; Zheng, S. *Polymer* **2008**, *49*, 3318. (t) Yi, F.; Zheng, S.; Liu, T. *J. Phys. Chem. B* **2009**, *113*, 11831.

(3) (a) Meng, F.; Zheng, S.; Zhang, W.; Li, H.; Liang, Q. *Macromolecules* **2006**, *39*, 711. (b) Meng, F.; Zheng, S.; Li, H.; Liang, Q.; Liu, T. *Macromolecules* **2006**, *39*, 5072. (c) Serrano, E.; Tercjak, A.; Kortaberria, G.; Pomposo, J. A.; Mecerreyes, D.; Zafeiropoulos, N. E.; Stamm, M.; Mondragon, I. *Macromolecules* **2006**, *39*, 2254. (d) Meng, F.; Zheng, S.; Liu, T. *Polymer* **2006**, *47*, 7590. (e) Sinturel, C.; Vayer, M.; Erre, R.; Amenitsch, H. *Macromolecules* **2007**, *40*, 2532. (f) Ocando, C.; Serrano, E.; Tercjak, A.; Pena, C.; Kortaberria, G.; Calberg, C.; Grignard, B.; Jerome, R.; Carrasco, P. M.; Mecerreyes, D.; Mondragon, I. *Macromolecules* **2007**, *40*, 4068. (g) Xu, Z.; Zheng, S. *Macromolecules* **2007**, *40*, 2548. (h) Meng, F.; Xu, Z.; Zheng, S. *Macromolecules* **2008**, *41*, 1411. (i) Fan, W.; Zheng, S. *Polymer* **2008**, *49*, 3157. (j) Fan, W.; Wang, L.; Zheng, S. *Macromolecules* **2009**, *42*, 327. (k) Ocando, C.; Tercjak, A.; Martín, M. D.; Ramos, J. A.; Campo, M.; Mondragon, I. *Macromolecules* **2009**, *42*, 6215.

(4) (a) Knop, A.; Scheib, W. *Chemistry and Application of Phenolic Resins*; Springer: Berlin, 1979. (b) Winkler, E. L.; Parker, J. A. *J. Macromol. Sci., Sci. Rev. Macromol. Chem.* **1971**, *C5*, 245. (c) Yamashita, Y.; Ouchi, K. *Carbon* **1981**, *19*, 89. (d) Fyfe, C. A.; Makinnon, M. S.; Rudin, A.; Tchir, W. J. *Macromolecules* **1983**, *16*, 1216. (e) Eckert, H.; Levendis, Y. A.; Flagan, R. C. *J. Phys. Chem.* **1988**, *92*, 5011. (f) Sonobe, N.; Kyotani, T.; Tomita, A. *Carbon* **1990**, *28*, 483. (g) Shindo, A.; Izumino, K. *Carbon* **1994**, *32*, 1233. (h) Manocha, L. M. *Carbon* **1994**, *32*, 213. (i) Wang, Z.; Lu, Z.; Huang, X.; Xue, R.; Chen, L. *Carbon* **1998**, *36*, 51. (j) Zhang, X.; Solomon, D. H. *Chem. Mater.* **1999**, *11*, 384.

(5) (a) Kosonen, H.; Ruokolainen, J.; Nyholm, P.; Ikkala, O. *Macromolecules* **2001**, *34*, 3046. (b) Valkama, S.; Nykaenen, A.; Kosonen, H.; Ramani, R.; Tuomisto, F.; Engelhardt, P.; ten Brinke, G.; Ikkala, O.; Ruokolainen, J. *Adv. Funct. Mater.* **2007**, *17*, 183. (c) Meng, F.; Yi, F.; Zheng, S. *J. Macromol. Sci., Part B: Phys.* **2008**, *47*, 450. (d) Kosonen, H.; Ruokolainen, J.; Torkkeli, M.; Serimaa, R.; Nyholm, P.; Ikkala, O. *Macromol. Chem. Phys.* **2002**, *203*, 388. (e) Zhang, F.; Meng, Y.; Gu, D.; Yan, Y.; Chen, Z.; Tu, B.; Zhao, D. *Chem. Mater.* **2006**, *18*, 5297. (f) Huang, Y.; Cai, H.; Yu, T.; Zhang, F.; Zhang, F.;

Meng, Y.; Gu, D.; Wan, Y.; Sun, X.; Tu, B.; Zhao, D. *Angew. Chem., Int. Ed.* **2007**, *46*, 1089. (g) Deng, Y.; Yu, T.; Wan, Y.; Shi, Y.; Meng, Y.; Gu, D.; Zhang, L.; Huang, Y.; Liu, C.; Wu, X.; Zhao, D. *J. Am. Chem. Soc.* **2007**, *127*, 1690.
(6) Wang, J.-S.; Matyjaszewski, K. *J. Am. Chem. Soc.* **1995**, *117*, 5614.
(7) Jnkova, K.; Chen, X.; Kops, J.; Batsberg, W. *Macromolecules* **1998**, *31*, 538.
(8) Zhong, Z.; Guo, Q. *Polymer* **1998**, *39*, 517.
(9) (a) Purcell, K. F.; Drago, R. S. *J. Am. Chem. Soc.* **1968**, *24*, 251. (b) Coleman, M. M.; Painter, P. C. *Appl. Spectrosc. Rev.* **1984**, *20*, 225. (c) Coleman, M. M.; Graf, J. F.; Painter, P. C. *Specific Interactions and the Miscibility of Polymer Blends*; Technomic Publishing: Lancaster, PA, 1991. (d) Coleman, M. M.; Painter, P. C. *Prog. Polym. Sci.* **1995**, *20*, 1.
(10) (a) Lu, H.; Zheng, S. *Polymer* **2003**, *44*, 4689. (b) Hu, L.; Lu, H.; Zheng, S. *J. Polym. Sci., Part B: Polym. Phys.* **2004**, *42*, 2567.
(11) (a) Patrick, J. W. In *Porosity in Carbons: Characterization and Applications*; Edward Arnold: London, 1995. (b) Lee, J.; Han, J.; Hyeon, T. *J. Mater. Chem.* **2004**, *14*, 478. (c) Kravchik, A. E.; Kukushkina, J. A.; Sokolov, V. V.; Tereshchenko, G. F. *Carbon* **2006**, *44*, 3263. (d) Jun, S.; Joo, S. H.; Ryoo, R.; Kruk, M.; Jaroniec, M.; Liu, Z.; Ohsuna, T.; Terasaki, O. *J. Am. Chem. Soc.* **2000**, *122*, 10712. (e) Gogotsi, Y.; Nikitin, A.; Ye, H.; Zhou, W.; Fischer, J. E.; Yi, B.; Foley, H. C.; Barsoum, M. W. *Nat. Mater.* **2003**, *2*, 591. (f) Yamazaki, M.; Kayama, M.; Ikeda, K.; Alii, T.; Ichihara, S. *Carbon* **2004**, *42*, 1641.